Journal of Crystal Growth 403 (2014) 124–127

Contents lists available at ScienceDirect

Journal of Crystal Growth

journal homepage: www.elsevier.com/locate/jcrysgro

Bulk properties of InN films determined by experiments and theory

M. Kumar [a,*,1], G. Baldissera [a], C. Persson [a,b], D.G.F. David [c], M.V.S. da Silva [c], J.A. Freitas Jr. [d], J.G. Tischler [d], J.F.D. Chubaci [e], M. Matsuoka [e], A. Ferreira da Silva [c,*]

[a] Department of Materials Science and Engineering, Royal Institute of Technology, SE-100 44 Stockholm, Sweden
[b] Department of Physics, University of Oslo, NO-0316 Oslo, Norway
[c] Instituto de Física, Universidade Federal da Bahia, Salvador, BA 40210-340, Brazil
[d] Naval Research Laboratory, Washington, DC 20375, USA
[e] Instituto de Física, Universidade de São Paulo, SP 05315-970, Brazil

ARTICLE INFO

Available online 9 June 2014

Keywords:
InN
Photoluminescence
Ion beam deposition
Density functional theory

ABSTRACT

Bulk properties of InN are determined by combining experimental and theoretical studies. In this work, we produced high quality InN film deposited on GaN templates by a modified ion beam assisted deposition technique confirmed by low temperature photoluminescence and absorption. The density of states, real and imaginary parts of the complex dielectric function and the absorption coefficient are calculated by means of first-principles beyond density-functional theory. The quasi-particle aspect is described in the framework of a quasi-particle method (the GW approximation). The calculated band-gap energy is ~0.8 eV whereas significance in the optical absorption occurs at ~1.2 eV, which are consistent with both luminescence and absorption results. The Bethe–Salpeter equation is utilized to model the two-particle exciton interactions, revealing a strong excitonic peak just below the absorption edge of InN.

1. Introduction

The optical and electronic properties of InN have drawn intensive research, mostly because of their potential applications for optoelectronic and electronic devices [1]. Fundamental properties of the material, such as its band-gap energy, are still not well established [2]. To date, there is an increasing interest in developing deposition techniques to yield high quality InN films for the fabrication of III-nitride based high-efficiency multi-junction solar cells, and high-frequency and high-power devices. However, there are major roadblocks preventing the full realization of these envisioned devices. In addition to the high concentration of extended defects, typical for heteroepitaxial deposition, challenges still remain due to the low In dissociation temperature, high incorporation of oxygen, and lack of conductivity type control [3]. Therefore, alternative deposition techniques to reduce these technical difficulties are highly desirable.

Theoretical studies of InN are usually based on density functional theory (DFT) [4–6], but there is uncertainty regarding the band gap values. It is well known that local density approximations (LDA) or generalized gradient approximations (GGA) severely underestimates the fundamental band gaps of semiconductors. For example, the reported band gap energies of InN with DFT/LDA or DFT/GGA are between 0.0 and −0.3 eV [4,5]. Quasi-particle corrections to the LDA change the bandgap to values between 0.6 and 0.8 eV [5,6].

We used the projector augmented wave (PAW) method within the DFT and in conjunction with Green's function and the screened Coulomb interaction approximation (GW_0) to obtain accurate band gap energies. In addition, the Bethe–Salpeter equation (BSE) is employed to analyze the two-particle exciton effect of the optical spectra. Combined investigations of experimental and theoretical studies reveal that the fundamental band-gap energy is ~0.8 eV. However, since the density of states (DOS) at the conduction band edge is small, the absorption is small in the energy region 0.8 – 1.2 eV and a clear onset to absorption occurs at ~1.2 eV. The BSE calculation reveals a strong excitonic peak just below the absorption edge of InN. Our theoretical results are compared with photoluminescence (PL) and absorption spectra for InN deposited on GaN templates by a modified ion beam assisted deposition (IBAD) technique.

2. Experimental details

Thin InN films were deposited at room temperature, 250 °C, or 395 °C by the modified ion beam assisted deposition (IBAD) on GaN/sapphire template substrates. The IBAD system consists of an

* Corresponding authors.
E-mail addresses: mukesh@kth.se (M. Kumar), ferreira.fis@gmail.com (A. Ferreira da Silva).
[1] Current affiliation: Environmental Remediation Materials Unit, National Institute for Materials Science, Ibaraki 305-0047, Japan.

http://dx.doi.org/10.1016/j.jcrysgro.2014.06.001
0022-0248/

electron-beam evaporator and a Kaufmann-type nitrogen ion gun in a vacuum chamber evacuated by a cryopump at base pressures below 10^{-4} Pa. The nitrogen ion energy of 100 eV and the evaporated 99.99% In metal reach simultaneously the substrate with an arrival rate ratio ARR(N/In) of 1.0, 1.5, 2.0, 2.5, or 3.0. ARR (N/In) is defined as the ratio of the flux of incident atomic nitrogen particles in the ion beam relative to the flux of evaporated indium atoms transported to the substrate. The thickness of the deposited films varied from 50 to 180 nm. Low temperature PL measurements were carried out using the 532 nm line of a doubled frequency Nd:Yag laser as the exciting source.

3. Computational details

All the calculations are performed using DFT by employing the PAW method as implemented in the Vienna ab initio simulation package (VASP) [7]. The atomic structure of InN is modeled by a fully relaxed wurtzite structure of 4 atoms ($C_{6v}^4 - P6_3mc$: space group number 186). The In-4*d* electrons are treated as valence electrons. The structure is relaxed using the local density approximation (LDA) with a $10\times10\times8$ k-mesh, until forces on the atoms were less than 12 meV Å^{-1}. The energy cut-off was taken to be 400 eV. The LDA with an on-site Coulomb correction (LDA+U) over *s* states of nitrogen, Us(N)$=-3$ eV is used to open the gap. The DOS, as well as the optical properties such as the frequency dependent dielectric function $\varepsilon(\omega)$ and the absorption coefficient $\alpha(\omega)$, are obtained with the use of a quasi-particle method (self-consistent GW_0) [8].

The dielectric functions were obtained from a partially self-consistent GW_0 approach using LDA wave functions, where Green's function *G* is updated iteratively, whereas the screened Coulomb potential, *W*, is kept fixed. The imaginary part $\varepsilon_2(\omega)$ of the dielectric function is calculated from the joint DOS and the optical momentum matrix in the long wave length $q=|\mathbf{k}'-\mathbf{k}|=0$ limit from the equation below [9]:

$$\varepsilon_2^{\alpha\beta}(\omega)=\frac{4\pi^2e^2}{\Omega}\lim_{q\to0}\frac{1}{q^2}\sum_{c,v,\mathbf{k}}2w_{\mathbf{k}}\delta(E_{c\mathbf{k}}-E_{v\mathbf{k}}-\omega)\langle u_{c\mathbf{k}+\mathbf{e}_\alpha q}|u_{v\mathbf{k}}\rangle\langle u_{c\mathbf{k}+\mathbf{e}_\beta q}|u_{v\mathbf{k}}\rangle,$$

where *e* is the electron charge, Ω is the primitive cell volume, $w_{\mathbf{k}}$ is the weight of $\mathbf{k}$-points, $\mathbf{e}_\alpha$ and $\mathbf{e}_\beta$ are the unit vectors for the three Cartesian directions. Indices *c* and *v* refer to CB and VB states respectively. $E_{j\mathbf{k}}$ is the single-electron energy state of band *j* at wave vector $\mathbf{k}$, and $u_{j\mathbf{k}}$ is the cell periodic part of the Bloch wave function corresponding to the eigenvalue $E_{c\mathbf{k}}$. The real part $\varepsilon_1(\omega)$ of the dielectric function is obtained from the Kramers–Kronig transformation [9]:

$$\varepsilon_1^{\alpha\beta}(\omega)=1+\frac{2}{\pi}P\int_0^\infty\frac{\varepsilon_2^{\alpha\beta}(\omega')\omega'}{\omega'^2-\omega^2+i\eta}d\omega',$$

where *P* is the principal value and η is an infinitesimal number. The absorption coefficient $\alpha(\omega)$ is obtained directly from the dielectric function by [9]

$$a(w)=(\sqrt{2\omega^2}/c)\cdot\left[\sqrt{\varepsilon_1(\omega)^2+\varepsilon_2(\omega)^2}-\varepsilon_1(\omega)\right]^{1/2},$$

where *c* is the speed of light.

It is important to note that the description of the excited particles, electron and hole, as quasi-particles is not sufficient. Therefore, the corresponding BSE [10] for the macroscopic polarization function is solved by applying the Tamm–Dancoff approximation [11], which is reliable in describing excitonic effects [12]. We follow standard computational procedures based on LDA+GW_0 self-consistent calculation as a base to solve the two-particle Schrodinger equation. The four valence and six conduction bands along with $10\times10\times8$ k-point grid is used to obtain the imaginary part $\varepsilon_2(\omega)$ of the dielectric function from the BSE [11] as

$$\varepsilon_2(\omega)=\frac{16\pi e^2}{\omega^2}\sum_{c,v}|\vec{\lambda}\cdot\langle v|\vec{\nu}|c\rangle|^2\delta(\omega-(E_c-E_v)),$$

where $\vec{\lambda}=\vec{A}/|A|$ is the polarization vector of the light, while $\vec{\nu}=i/\hbar[H,\vec{r}]$ is the single-particle velocity operator, *v* and *c* are valence and conduction states.

4. Results and discussion

4.1. Photoluminescence

Luminescence measurements were carried out at 4.2 K using the 532 nm line of a doubled frequency Nd:Yag laser. The sample emission was dispersed and analyzed by a double spectrometer fitted with 1 μm blazed gratings and a LN_2-cooled Ge detector and/or with an InSb detector. Intense and sharp single emission bands were observed from all measured samples. Fig. 1 shows the PL spectra of three InN films, with thicknesses of 50 and 80 nm, deposited at 250 and 395 °C. One can see that the full width at half-maximum and the peak position are between 31 and 36 meV and 0.76 and 0.77 eV, respectively. These results indicate that this technique can reproducibly deposit high quality thin films. Note that the Sample-c, deposited at 395 °C, has relatively larger peak intensity. This is consistent with lower background concentration of non-radiative recombination centers.

4.2. Density of states

The total and partial density of states for wurtzite InN is shown in Fig. 2. The N *p*-states are the ones which have higher contribution in the valence band region. Nevertheless, the conduction band is formed by comparable contributions from all the In and the N states. Our calculated direct band gap of 0.75 eV with LDA+U/$scGW_0$ scheme is in good agreement with reported experimental measurements [2]. Similarly to GaN, the cation-*d* states play an important role in InN. LDA underestimates the self-interaction of the localized *d*-states, and in InN the LDA binding energy of the

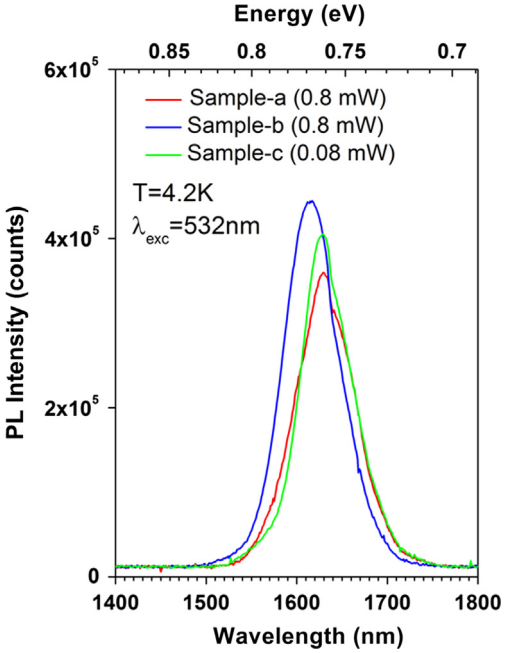

Fig. 1. Photoluminescence spectrum of three InN films deposited with ARR(N/In)=2.0 on GaN/sapphire substrate at 395 °C. Samples "a" and "b" were deposited at 250 °C while sample "c" was deposited at 395 °C.

d-states is ~3–4 eV, which is too small when compared to photo-emission experimental results. As a result, the LDA error affects the calculated hybridization between In-3*d* and N-2*s* in InN. Moreover, the cation-*d* anion-*s* hybridization creates an additional N-2*p*-like state within the In-*d* band [13]. The DOS at the conduction band edge is small, and this has an impact on the optical properties of InN.

4.3. Dielectric function of InN

The complex dielectric function $\varepsilon(\omega)$ is the main optical characteristic for a semiconductor. Fig. 3(a) shows the real $\varepsilon_1(\omega)$ and imaginary part $\varepsilon_2(\omega)$ of the dielectric function calculated with the scGW$_0$ approximation. A high frequency dielectric constant of $\varepsilon_\infty=6$ is estimated, which is close to values found in the literature ($\varepsilon_\infty=8$) [12]. On the other hand, the imaginary part shows a threshold in the energy around 1 eV. Fig. 3(b) shows the imaginary part of the dielectric function $\varepsilon_2(\omega)$ obtained from scGW$_0$ and BSE methods respectively. One can observe a strong excitonic peak E_{ex}~0.65 eV just below the absorption edge. This is in good agreement with literature values (~0.65 eV) reported for InN [12]. It is worth to notice that many details from the BSE spectra cannot be identified and moreover, it is not as smooth as the scGWo spectra. This occurs because a very large **k**-mesh is required to properly calculate the dielectric constant under this approximation, which is computationally too costly.

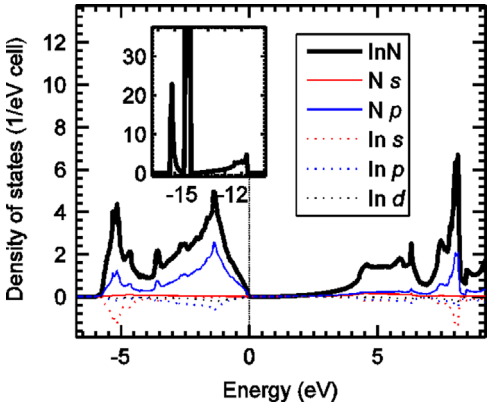

Fig. 2. The total and partial density of states for wurtzite InN. Inset shows some sharp peaks well below 15 eV from VBM.

4.4. Absorption coefficient of InN

Fig. 4 shows the absorption coefficient α (ω) of InN. The absorption spectra in the range from 0 to 10 eV calculated with the scGW0 method is shown in Fig. 4a. Here, we present the average polarization-independent absorption. Fig. 4(a) shows that absorption occurs at ~1.2 eV, and the intensity increases in the low energy region. Inset shows a graph of $(\alpha \times E)2$ vs. energy, in the band gap region. Its linear behavior indicates a direct valence band to conduction band transition.

The experimental absorption coefficient as a function of energy was obtained from a 160 nm InN film deposited on a 4.3 μm thick GaN/Sapphire template, by optical spectroscopy. As the surface of the sample was rough, only transmission spectra covering the range of 300 nm to 2200 nm were obtained. In order to remove the interferences resulting from multiple reflections inside the

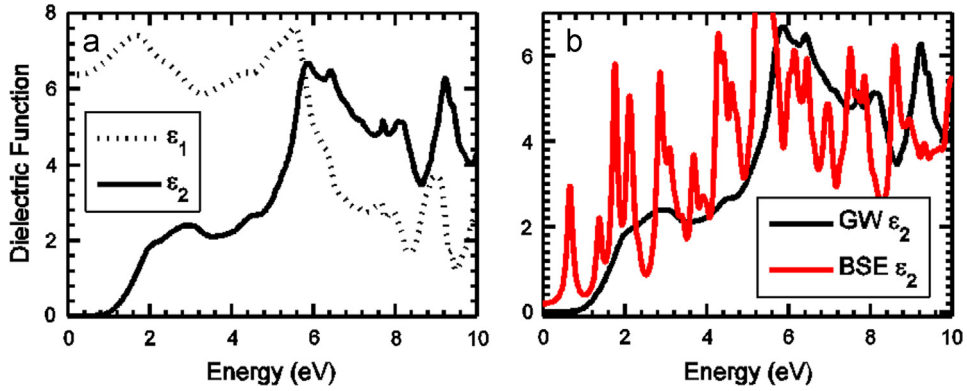

Fig. 3. Dielectric function $\varepsilon(\omega)$ of InN, (a) Calculated real $\varepsilon_1(\omega)$and imaginary part $\varepsilon_2(\omega)$ of dielectric functions from scGW$_0$ approximation, (b) comparative behaviors of imaginary part $\varepsilon_2(\omega)$ calculated with scGW$_0$ and BSE methods. One can observe a strong excitonic peak E_{ex} ~0.65 eV just below the absorption edge.

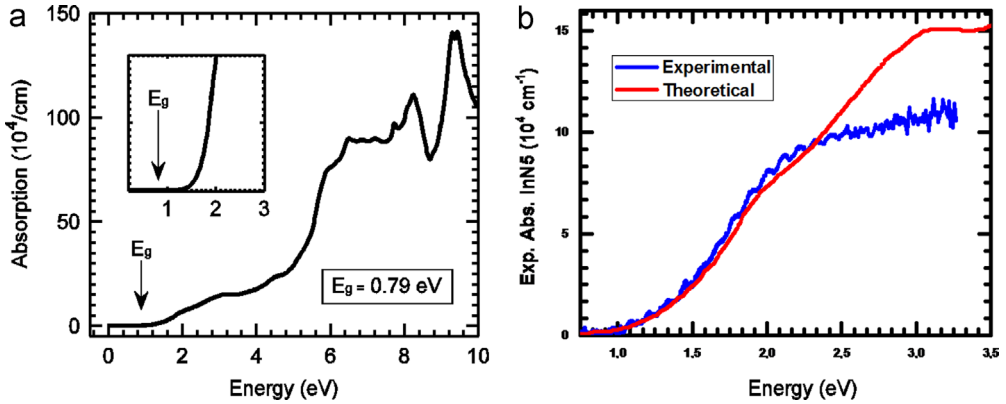

Fig. 4. The optical absorption coefficient α (ω) of InN. Calculated spectra from single particle interaction (scGW0) in the range from 0 to 10 eV, inset figure shows a graph of $(\alpha \times E)^2$ vs. energy to estimate the gap value, which is 0.79 eV. (b) Experimental absorption coefficient of an InN sample fabricated by IBAD compared with the calculated spectra in the range from 0 to 3.5 eV. One can notice a good agreement between experiments and theory.

GaN film, a model of these interferences was used to subtract their contribution to the experimental spectra. Fig. 4(b) shows a comparison between experimental and theoretical absorption spectra. The agreement is fairly good as the experimental gap is found around 1 eV, close to the theoretical gap. The two spectra reveal a similar profile and the absorption coefficients are found very close, up to 2.5 eV.

5. Summary

In conclusion, we present optical properties of InN within the framework of experimental measurements and theoretical calculations. The modified ion beam assisted deposition technique was used to grow high quality thin InN film. The DOS, absorption coefficients, and the real and imaginary parts of the dielectric functions of InN are studied theoretically by employing the projector augmented wave (PAW) method within the $scGW_0$ approximation. Combined investigations of experimental and theoretical studies reveal that the fundamental band-gap energy is $\sim$0.8 eV whereas a clear onset to absorption occurs at $\sim$1.2 eV. The BSE calculation reveals a strong excitonic peak just below the absorption edge of InN.

Acknowledgments

The authors acknowledge the financial support of the Brazilian agencies FAPESB/PRONEX and CNPq, the Swedish Research Council (VR), and Norwegian Research Council (NFR). We acknowledge access to HPC centers NSC and USIT for high-performance computing resources via SNIC/SNAC, Matter network and NOTUR. The experimental work was part of an ONR/IF-USP NICOP program initiated by the Brazilian PI Prof. José Roberto Leite.

References

[1] A.G. Bhuiyan, A. Hashimota, A. Yamamoto, J. Appl. Phys. 94 (2003) 2779;
T.D. Veal, C.F. McConville, W.J. Schaff (Eds.), Indium Nitride and Related Alloys, CRC Press W * J Taylor & Francis Group, Boca Raton, London, New York, 2009.
[2] T.L. Tansley, C.P. Foley, J. Appl. Phys. 59 (1986) 3241;
J. Wu, et al., Appl. Phys. Lett. 80 (2002) 3967;
T. Inushima, et al., J. Cryst. Growth 227–228 (2001) 481.
[3] E. Trybus, G. Namkoong, W. Henderson, S. Burnham, W.A. Doolittle, M. Cheung, A. Cartwright, J. Cryst. Growth 288 (2006) 218.
[4] N.E. Christensen, I. Gorczyca, Phys. Rev. B 50 (1994) 4397;
C. Stampfl, C.G. Van de Walle, Phys. Rev. B 59 (1999) 5521.
[5] U. Grossner, J. Furthmüller, F. Bechstedt, Phys. Rev. B 58 (1998) R1722;
F. Bechstedt, J. Furthmüller, J. Cryst. Growth 246 (2002) 315.
[6] C. Persson, A. Ferreira da Silva, J. Cryst. Growth 305 (2007) 408 (J. Phys.: Condens. Matter 13, (2001) 8945).
[7] G. Kresse, J. Furthmüller, Phys. Rev. B 54 (1996) 11169 (Comput. Mater. Sci. 6 (1996) 15).
[8] P.P. Gonzalez – Horrero, et al., Appl. Phys. Lett. 96 (2010) 061909;
M. Gajdos, K. Hummer, G. Kresse, J. Furthmuller, F. Brechstedt, Phys. Rev. B 73 (2006) 45112.
[9] M. Dou, G. Baldissera, C. Persson, J. Cryst. Growth 350 (2012) 17;
M. Kumar, H. Zhao, C. Persson, Semicond. Sci. Technol. 28 (2013) 065003.
[10] L.J. Sham, T.M. Rice, Phys. Rev. 144 (1966) 708;
W. Hanke, L.J. Sham, Phys. Rev. Lett. 43 (1979) 387.
[11] M. Rohlfing, S.G. Louie, Phys. Rev. B 62 (2000) 4927;
G. Onida, L. Reining, A. Rubio, Rev. Mod. Phys. 74 (2002) 601.
[12] L. Yang, Phys. Rev. B 83 (2011) 085405;
F. Fuchs, C. Rodl, A. Schleife, F. Bechstedt, Phys. Rev. B 78 (2008) 085103.
[13] C. Persson, A. Ferreira da Silva, in: M. Razeghi, M. Henini (Eds.), Optoelectronic Devices: III-Nitrides, Elsevier Advanced Technology, London, ISBN 0-08-044426-12004, pp. 479–559.